

## Effect of Grid Geometry on the Scale-by-scale Budget of Decaying Grid Turbulence

P. Lavoie, R. A. Antonia and L. Djenidi

Discipline of Mechanical Engineering  
University of Newcastle, Callaghan, NSW, 2308 AUSTRALIA

### Abstract

The approximately homogeneous, isotropic turbulence (HIT) produced by three grids with different geometries was measured over the range  $30 \leq x/M \leq 80$ . The scale-by-scale budget of decaying grid turbulence obtained from the transport equation for  $\langle (\delta q)^2 \rangle$  is used to study the effect of grid geometry in an attempt to quantify the influence of initial conditions of the turbulence decay. Although  $R_\lambda$  is too small for a scaling range to exist, the initial conditions show negligible effect on scales smaller than  $\lambda$ . The solidity of the grid influences only the very large scales. The shape of the grid elements can significantly affect the overall shape of the inhomogeneous term in the transport equation for  $\langle (\delta q)^2 \rangle$ .

### Introduction

Theoretical studies of decaying homogeneous, isotropic turbulence (HIT) have classically eliminated initial conditions from the problem with the assumption of infinite Reynolds number and invoking Kolmogorov's theory [12], although early presentations of the theory included a discussion of their possible effect on the decay [5]. Initial condition effects remained absent from HIT theory, which is the basis of most modern turbulence models, despite experimental and, more recently, DNS results that supported the importance of initial conditions via the unexplained wide scatter in  $m$ , the decay exponent [8, 10, 16].

Theoretical work by George [9], herein referred to as G92, argues for the importance of initial conditions and derives a self-similar theory for HIT that includes the effect of initial conditions and applies at finite Reynolds number. Although the derivation of the theory is strictly correct and some of its parts are supported by experimental and numerical data [2, 3, 17], certain aspects of the theory are argued to have no physical basis [9, 15]. G92 expects that the decay exponent will change with initial conditions. However, the analysis of Speziale and Bernard [15], referred herein as SB, predicts a universal decay that is reached asymptotically with time. Their analysis shows that the scatter in previously reported  $m$  could be due to some experimental data having been sampled in the transition zone prior to the universal decay state.

Alternatively, Mohamed and LaRue [13] suggested the scatter could be due to inconsistencies in the way different authors fitted the power-law to their respective measurements. These authors then proposed a procedure to estimate the parameters of the power-law, which they argued to be consistent and rigorous. When this was applied to their and other previously published data, they found a reduction in the scatter that pointed to a weak or non-existent dependence on initial conditions. However, the decay exponent thus obtained,  $m = -1.3$ , is significantly different from the value  $-1$  predicted by classical theories [5, 10].

As highlighted by this discussion of references [9, 13, 15], there remains much confusion and controversy regarding the actual cause of the scatter reported for  $m$ . Furthermore, George *et al.* [10] and Mohamed and LaRue [13] showed that the esti-

mation of  $m$  includes sizable uncertainties, which suggests that this variable may not be sensitive enough to show the effects of initial conditions on decaying HIT clearly. The difficulty with the study of initial conditions is that neither the initial conditions themselves nor their effects are easily quantifiable. This is particularly true in experimental work where the initial energy distribution over the turbulent scales can hardly be controlled or measured. This also makes comparisons between experimental and numerical results very difficult. It is the purpose of this paper to show that the scale-by-scale budget of the turbulence generated by three grids of different geometry can be used to quantify in a non-ambiguous manner the effect that initial conditions have on the approximately homogeneous, isotropic turbulence generated by these grids.

### Background

Grid turbulence provides a good approximation of decaying HIT and offers a direct measure of the mean dissipation rate from the turbulence kinetic energy decay, viz.

$$\langle \epsilon \rangle_d = -\frac{U}{2} \frac{d \langle q^2 \rangle}{dx}. \quad (1)$$

Danaila *et al.* [7] revisited the classical Kolmogorov "four-fifths law" [11] which relates the second- and third-order structure functions, viz.

$$-\langle (\delta u)^3 \rangle + 6\nu \frac{d}{dr} \langle (\delta u)^2 \rangle = \frac{4}{5} \langle \epsilon \rangle r, \quad (2)$$

where  $\delta u \equiv u(x+r) - u(x)$  is the difference in streamwise velocity fluctuations between two points separated by a distance  $r$  along the streamwise directions,  $\langle \epsilon \rangle$  is the mean kinetic energy dissipation rate and  $\langle \rangle$  denote an ensemble average. It is well known that equation (2) is only balanced for very small separations, typically of the order of a few Kolmogorov lengths,  $\eta \equiv \nu^{3/4} \langle \epsilon \rangle^{-1/4}$ , for the small and intermediate Reynolds numbers obtained in most experiments. In an attempt to study the effect of large-scale inhomogeneities on the small scales of turbulence, Danaila *et al.* [7] obtained a transport equation for  $\langle (\delta q)^2 \rangle$  from the Navier-Stokes equation for decaying grid turbulence, viz.

$$-\langle (\delta u) (\delta q)^2 \rangle + 2\nu \frac{d}{dr} \langle (\delta q)^2 \rangle - \frac{U}{r^2} \int_0^r s^2 \frac{\partial}{\partial x} \langle (\delta q)^2 \rangle ds = \frac{4}{3} \langle \epsilon \rangle r, \quad (3)$$

where  $\langle (\delta q)^2 \rangle \equiv \langle (\delta u)^2 \rangle + \langle (\delta v)^2 \rangle + \langle (\delta w)^2 \rangle$  and  $s$  is a dummy variable. Equation (3) is an extension of equation (2) with the addition of an inhomogeneity term. Also, the former takes into account the three velocity components, instead of only  $u$  in equation (2). It is important to note here that the inhomogeneous term in equation (3) is a consequence of the streamwise decay of the turbulence and that, for box turbulence

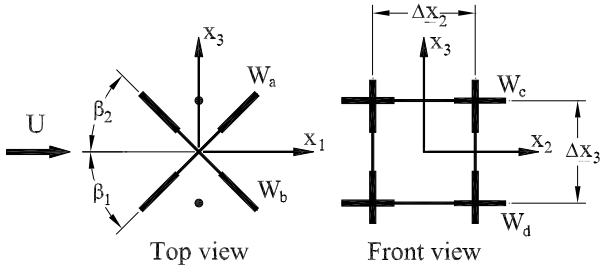


Figure 1: One-component vorticity probe.  $\Delta y \simeq 1.0$  mm,  $\Delta z \simeq 1.3$  mm,  $\beta_1 \simeq \beta_2 \simeq 45^\circ$ . All wires have a diameter of  $2.5 \mu\text{m}$  and were etched from Wollaston (Pt-10% Rh) material to a length of approximately 0.5 mm.

where there is no mean flow, it would take the form of a time-wise decay [14]. An important feature of equation (3) is that it can be used as a scale-by-scale budget of the turbulence [1, 6].

Following G92, Antonia *et al.* [3] derived the conditions for which equation 3 satisfied similarity. Their analysis yielded the following self-similar forms for the second- and third-order structure functions,

$$\langle (\delta q)^2 \rangle = \langle q^2 \rangle f\left(\frac{r}{\lambda}\right) \quad (4)$$

and

$$-\langle (\delta u)(\delta q)^2 \rangle = \left[ \frac{\langle q^2 \rangle^{3/2}}{3^{1/2} R_\lambda} \right] g\left(\frac{r}{\lambda}\right), \quad (5)$$

respectively, where  $\lambda$  is the Taylor microscale, defined here as

$$\lambda^2 = 5\nu \frac{\langle q^2 \rangle}{\langle \epsilon \rangle_d}, \quad (6)$$

and  $R_\lambda$  is taken as

$$R_\lambda = \frac{\langle q^2 \rangle^{1/2} \lambda}{3^{1/2} \nu}. \quad (7)$$

Under these conditions,  $f$  and  $g$  are independent of  $x$  and the turbulence decays following a power-law of the form

$$\langle q^2 \rangle = a \left( \frac{x}{M} - \frac{x_o}{M} \right)^m, \quad (8)$$

where  $x_o/M$  is the virtual origin,  $m$  is the power-law exponent and  $a$  is a constant of proportionality. Detailed derivation and discussion of this theory can be found in [3].

When equations (1), (4), (5) and (8) were applied to equation (3), Antonia *et al.* [3] obtained a self-similar form for the scale-by-scale budget, viz.

$$g + 2f' - \left[ \frac{5\Gamma_1}{m} \left(\frac{r}{\lambda}\right)^{-2} - 10\Gamma_2 \left(\frac{r}{\lambda}\right)^{-2} \right] = \frac{20}{3} \left(\frac{r}{\lambda}\right), \quad (9)$$

where  $\Gamma_1$  and  $\Gamma_2$  are given by

$$\Gamma_1 \equiv \int_0^{r/\lambda} \left(\frac{s}{\lambda}\right)^3 f' d\left(\frac{s}{\lambda}\right) \quad (10)$$

$$\Gamma_2 \equiv \int_0^{r/\lambda} \left(\frac{s}{\lambda}\right)^2 f d\left(\frac{s}{\lambda}\right). \quad (11)$$

Equation (9) can be written symbolically as  $A + B + [\text{INH}] = C$ , where INH represents the total streamwise inhomogeneous term.

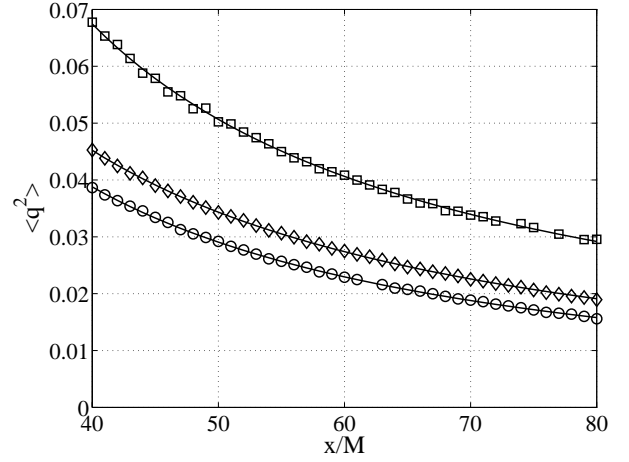


Figure 2: Streamwise variation of  $\langle q^2 \rangle$  behind the three grids (Sq35,  $\square$ ; Rd35,  $\circ$ ; Rd44,  $\diamond$ ) compared to the fitted power-laws (fitting parameters summarized in table 1).

### Experimental Details

The measurements presented here were made with a one-component vorticity probe, which consists of parallel wires and a X-wire. Figure 1 gives a schematic of the probe with typical dimensions. A vorticity probe was used to obtain more complete measurements of the turbulence behind the grids. Vorticity results are however not presented here. The wires were operated with in-house constant-temperature circuits at an overheat ratio of 0.5. The signals were then amplified and low-pass filtered at a cut-off frequency of  $f_c$ , which varied depending on the grid and  $x/M$ .  $f_c$  was selected to correspond to the onset of electronic noise and was of the order of  $f_k \equiv U/2\pi\eta$ , the Kolmogorov frequency. The signals were sampled at a frequency  $f_s \geq 2f_c$  and digitized with a 16 bit A/D converter for a duration of 60 to 300 seconds.

Three biplane grids were used, all with the same mesh size  $M = 24.76$  mm. The geometry of the grids was varied by changing the shape of the bars cross-section and the solidity of the grid. The first grid, Sq35, was made with square bars and solidity  $\sigma \equiv d/M(2 - d/M) = 0.35$ . The other two grids, Rd35 and Rd44, were both manufactured with round rods but with  $\sigma = 0.35$  and  $\sigma = 0.44$ , respectively. The grids were placed downstream of the contraction (area ratio of 9:1) of an open-circuit wind tunnel. The length of the working section was 2.4 m and its cross-sectional area at the contraction was 350 mm  $\times$  350 mm (the floor of the tunnel was slightly inclined to provide zero pressure gradient). The probe was traversed along the centerline of the working section. Measurements were made between  $x/M = 30$  and  $x/M = 80$  in steps of one mesh length with a mean velocity  $U = 6.4$  m/s ( $Re_M = UM/\nu \approx 10,400$ ) for all three grids. The mean turbulent statistics obtained with the vorticity probe were corrected for spatial resolution following the method described in Zhu and Antonia [18]. The flow was assumed to be axisymmetric so that  $v$  and  $w$  statistics are taken to be equal. The measurements of  $w$  and  $uw$  correlations were taken from the X-wire, while the average of the two single wires was used for  $u$ .

### Results

The decay exponent for each grid was obtained here by fitting equation (8) in the range  $40 \leq x/M \leq 80$  with the MatLab routine NLINFIT. Initial estimates for  $a$  and  $m$  were obtained by assuming  $x_o/M = 0$  and applying a linear regression to  $\log(\langle q^2 \rangle)$

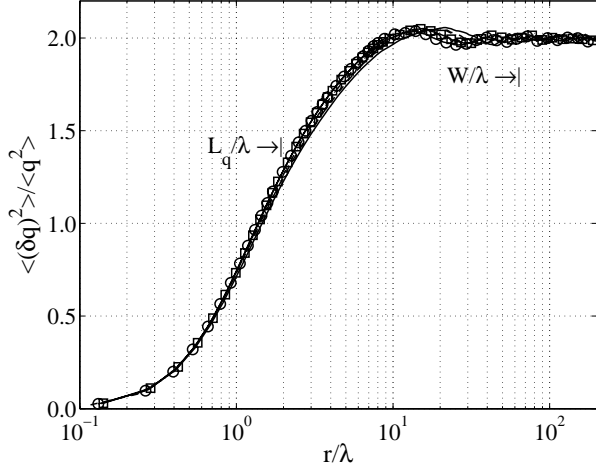


Figure 3: Second-order turbulent energy structure function for *Rd44*.  $x/M = 30$ , —;  $x/M = 40$ , - - -;  $x/M = 50$ , - · - ·;  $x/M = 60$ , ·····;  $x/M = 70$ , □-□;  $x/M = 80$ , -○-○.

Grid	$m$	$\frac{x_o}{M}$	$\frac{\langle u^2 \rangle}{\langle w^2 \rangle}$	$R_\lambda$	$\lambda$ mm	$L_q$ mm	$\eta$ mm
<i>Sq35</i>	-1.13	3	1.48	41.1	5.36	13.7	0.42
<i>Rd35</i>	-1.31	0	1.40	30.0	5.23	10.2	0.48
<i>Rd44</i>	-1.28	0	1.39	33.4	5.32	10.8	0.47

Table 1: Decay law parameters and other basic turbulence characteristics obtained at  $x/M = 60$  for the three grids.

vs.  $\log(x/M)$ . The power-laws obtained are compared graphically in figure 2 to the measured  $\langle q^2 \rangle$ . Figure 3 presents  $\langle (\delta q)^2 \rangle$  normalized according to G92 for *Rd44* and shows that similarity is only reached approximately for  $x/M \geq 40$ . The plots for *Sq35* and *Rd35* lead to the same conclusions and are not shown here. The three criteria suggested by Mohamed and LaRue [13] were met before  $x/M = 40$ ; namely  $S_u = \langle u^3 \rangle / \langle u^2 \rangle^{3/2}$  was zero,  $S_{\partial u / \partial x} = \langle (\partial u / \partial x)^3 \rangle / \langle (\partial u / \partial x)^2 \rangle^{3/2}$  was constant and  $\langle \epsilon \rangle_{iso} \equiv 15v \langle (\partial u / \partial x)^2 \rangle$  was equal to  $\langle \epsilon \rangle_d$  within 10%. Note here that the results of the scale-by-scale budgets presented are insensitive to errors in  $m$  and therefore the method of determining  $m$  used was deemed sufficient for the purposes of this paper.

We shall concentrate our analysis to the measurements obtained at  $x/M = 60$  since the results do not change significantly with location for  $40 \leq x/M \leq 80$ , due to the quasi-self-similar turbulence decay. The location  $x/M = 60$  presents a good compromise between probe resolution, which improves with increasing  $x/M$ , the degradation of the signal-to-noise ratio with  $x/M$  and increasing confinement of the turbulence due to the finite width of the tunnel. A few basic quantities measured at this location are summarized in table 1. Note that the integral length scale  $L_q$  is defined here as

$$L_q = \frac{1}{\langle q^2 \rangle} \int_0^{r_o} B_{q,q}(r) dr, \quad (12)$$

where  $B_{q,q}$  is calculated here as

$$B_{q,q} = \langle q(x)q(x+r) \rangle = \langle u(x)u(x+r) \rangle + 2\langle w(x)w(x+r) \rangle \quad (13)$$

and  $r_o$  is the first zero crossing of  $B_{q,q}$ .

Figure 4 compares the function  $f(r/\lambda)$  measured behind each grid at  $x/M = 60$ . The ratio  $W/\lambda$ , where  $W$  is the width of

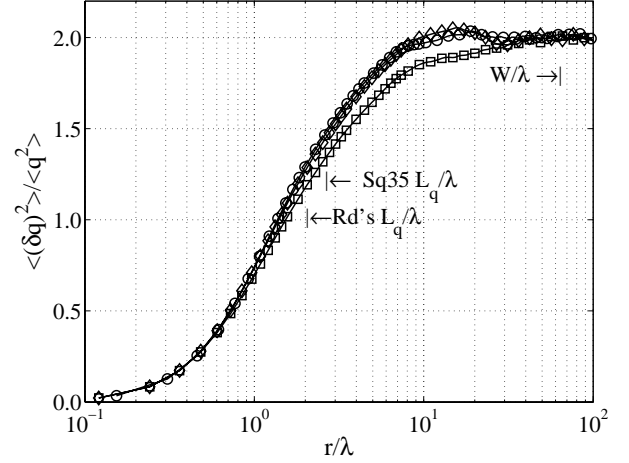


Figure 4: Second-order turbulent energy structure function measured at  $x/M = 60$  behind three grid geometries: *Sq35*, □; *Rd35*, ○; *Rd44*, ◇. Indicated are the ratios  $W/\lambda$ , which is approximately equal for the three grids at  $x/M = 60$ , and  $L_q/\lambda$ , which is roughly equal for *Rd35* and *Rd44*.

the tunnel, is included to provide an indication of the values of  $r/\lambda$  that may be affected by the size of the tunnel. For  $r/\lambda < 1$ , the normalized structure functions are nearly equal for the three grids. In the range  $1 \leq r/\lambda \leq 7$ , the difference between *Rd35* and *Rd44* is within 1.4%, which is the estimated statistical uncertainty, while *Sq35* shows a clear departure from the two round-rod grids by  $r/\lambda = 1$ . Figure 4 establishes that  $f(r/\lambda)$  for *Sq35* approaches the asymptotic value of 2 monotonically from below. This is contrasted to *Rd35* and *Rd44* for which  $f(r/\lambda)$  overshoots the asymptote before it settles to 2 as  $r/\lambda \rightarrow \infty$ . This overshoot for the round-rod grids suggests that the large turbulent scales behind these two grids are more periodic in nature than those for *Sq35*. The stronger overshoot and oscillations at large separations outside the measurement scatter for *Rd44* imply that the periodic structures of *Rd44* are stronger than for *Rd35*.

The scale-by-scale budgets compensated with  $(r/\lambda)$  for the three grids are compared in figure 5. As shown, the left-side of equation (9) equals  $20/3 \pm 10\%$  at all separations. In the range  $r/\lambda < 1$ , the balance is very sensitive to inaccuracies in the estimate of  $\lambda$ , while at larger separations, the main uncertainty comes from the statistical convergence of  $g(r/\lambda)$ . For the current experiments there is no separation between the scales responsible for the dissipation of turbulence and the scales affected by INH, which is not surprising given the low  $R_\lambda$ . It is also clear that INH does not differ significantly for the three grids up to about  $r/\lambda = 1$ . While the inhomogeneous term for *Sq35* deviates from that of the two round-rod grids for  $r/\lambda \geq 1$ , there is little difference between *Rd35* and *Rd44* until  $r/\lambda > 8$ . These observations indicate that the three grid geometries studied here have little effect on the turbulent scales ranging from  $\eta$  to  $\lambda$ . However, the shape of the bar cross-section show an influence on scales as small as  $\lambda$ . The solidity of the round-rod grids appears to impact only on scales much larger than  $L_q$ .

## Concluding Comments

The effect of grid geometry was studied using the turbulent energy structure function and the related scale-by-scale budget. The small Reynolds numbers of the current experiment prohibited the formation of a proper separation between the scales responsible for the turbulence dissipation and those affected by the inhomogeneity of the flow. Despite the low  $R_\lambda$ , the three

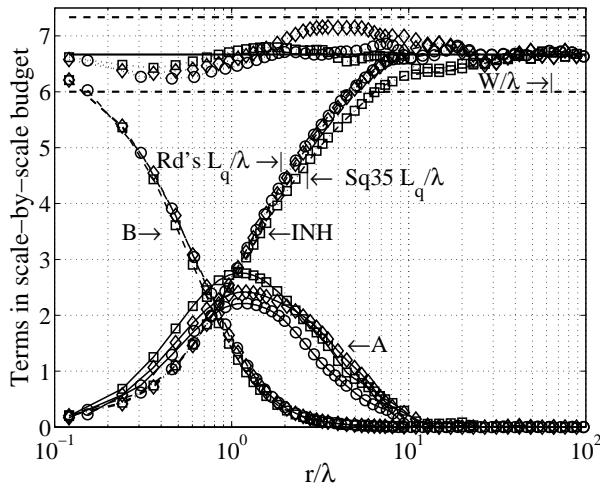


Figure 5: Comparison between the energy budget behind the three grids ( $Sq35$ ,  $\square$ ;  $Rd35$ ,  $\circ$ ;  $Rd44$ ,  $\diamond$ ) at  $x/M = 60$ .  $A(r/\lambda)^{-1}$ , —;  $B(r/\lambda)^{-1}$ , ---;  $INH(r/\lambda)^{-1}$ , - · - ·;  $(A+B+INH)(r/\lambda)^{-1}$ , ······. The thick horizontal line is at  $20/3$  and the horizontal dotted lines represent  $\pm 10\%$ . Also indicated for reference are the ratios  $W/\lambda$  and  $L_q/\lambda$ .

different grid geometries studied here had little effect on scales ranging between  $\eta$  and  $\lambda$ . Overall, the shape of the bars exhibited a stronger influence on the energy containing scales than the grid solidity. This latter parameter was only important for  $r/\lambda \geq 8$  and mainly affected the periodicity of large organized structures. The questions of how the grid geometry produces different turbulent states and how these affect important parameters, such as the power-law energy decay exponent, remain however undetermined.

A detailed study of the turbulence from very close to the grid up to the quasi-self-similar region is required to answer the first of these questions. The complexity of the flow field and reduced scales of the turbulence near the grid make hot-wire measurements more difficult and uncertain. Other methods of flow measurements, such as PIV [4], can however be employed to corroborate and complement hot-wire data.

A more detailed understanding of the effect of grid geometry on approximately homogeneous, isotropic turbulence is the subject of continued work. The scale-by-scale budget for grid turbulence, which was shown to capture quantitatively the effect the grid-geometry in this paper, should prove to be an invaluable tool in the study of decaying HIT.

#### Acknowledgements

The authors would like to acknowledge the support of the Australian Research Council and the Australian Government.

#### References

[1] Antonia, R. A. and Burattini, P., Small scale turbulence: how universal is it?, in *15th Australasian Fluid Mechanics Conference*, University of Sydney, 2004.

[2] Antonia, R. A. and Orlandi, P., Similarity of decaying isotropic turbulence with a passive scalar, *J. Fluid Mech.*, **505**, 2004, 123–151.

[3] Antonia, R. A., Smalley, R. J., Zhou, T., Anselmet, F. and Danaila, L., Similarity of energy structure functions in de-

caying homogeneous isotropic turbulence, *J. Fluid Mech.*, **487**, 2003, 245–269.

[4] Avallone, G., De Gregorio, F. and Romano, G. P., PIV measurements in grid turbulence, in *5th International Symposium on Particle Image Velocimetry*, Busan, Korea, September 22–24, 2003.

[5] Batchelor, G. K., *The Theory of Homogeneous Turbulence*, Cambridge University Press, 1953.

[6] Burattini, P., Antonia, R. A. and Rajagopalan, S., Effect of initial conditions on the far field of a round jet, in *15th Australasian Fluid Mechanics Conference*, University of Sydney, 2004.

[7] Danaila, L., Anselmet, F. and Antonia, R. A., An overview of the effect of large-scale inhomogeneities on small-scale turbulence, *Phys. Fluids*, **14**, 2002, 2475–2484.

[8] Gad-el-Hak, M. and Corrsin, S., Measurements of the nearly isotropic turbulence behind a uniform jet grid, *J. Fluid Mech.*, **62**, 1974, 115–143.

[9] George, W. K., The decay of homogeneous isotropic turbulence, *Phys. Fluids*, **4**, 1992, 1492–1509.

[10] George, W. K., Wang, H., Wollbald, C. and Johansson, T. G., Homogeneous turbulence and its relation to realizable flows, in *14th Australasian Fluid Mechanics Conference*, Adelaide University, 2001, 41–48, 41–48.

[11] Kolmogorov, A., Dissipation of energy in locally isotropic turbulence, *C. R. Acad. Sci. U.R.S.S.*, **32**, 1941, 16–18.

[12] Kolmogorov, A., The local structure of turbulence in incompressible viscous fluid for very large Reynolds number, *C. R. Acad. Sci. U.R.S.S.*, **30**, 1941, 301–305.

[13] Mohamed, M. S. and LaRue, J. C., The decay power law in grid-generated turbulence, *J. Fluid Mech.*, **219**, 1990, 195–214.

[14] Pope, S. B., *Turbulent Flows*, Cambridge University Press, 2000.

[15] Speziale, C. G. and Bernard, P. S., The energy decay in self-preserving isotropic turbulence revisited, *J. Fluid Mech.*, **241**, 1992, 645–667.

[16] Uberoi, M. S. and Wallis, S., Effect of grid geometry on turbulence decay, *Phys. Fluids*, **10**, 1967, 1216–1224.

[17] Wang, H. and George, W. K., The integral scale in homogeneous isotropic turbulence, *J. Fluid Mech.*, **459**, 2002, 429–443.

[18] Zhu, Y. and Antonia, R. A., The spatial resolution of hot-wire arrays for the measurement of small-scale turbulence, *Meas. Sci. Tech.*, **7**, 1996, 1349–1359.